CLIMATOLOGY

Contemporary ice sheet thinning drives subglacial groundwater exfiltration with potential feedbacks on glacier flow

Alexander A. Robel[1]*, Shi J. Sim[1], Colin Meyer[2], Matthew R. Siegfried[3], Chloe D. Gustafson[4]

Observations indicate that groundwater-laden sedimentary aquifers are extensive beneath large portions of the Greenland and Antarctic ice sheets. A reduction in the mechanical loading of aquifers is known to lead to groundwater exfiltration, a discharge of groundwater from the aquifer. Here, we provide a simple expression predicting exfiltration rates under a thinning ice sheet. Using contemporary satellite altimetry observations, we predict that exfiltration rates may reach tens to hundreds of millimeters per year under the fastest thinning parts of the Antarctic Ice Sheet. In parts of West Antarctica, predicted rates of exfiltration would cause the total subglacial water discharge rate to be nearly double what is currently predicted from subglacial basal melting alone. Continued Antarctic Ice Sheet thinning into the future guarantees that the rate and potential importance of exfiltration will only continue to grow. Such an increase in warm, nutrient-laden subglacial water discharge would cause changes in ice sliding, melt of basal ice and marine biological communities.

INTRODUCTION

Water permeates the environment beneath ice sheets. This subglacial water can form complex drainage systems at the ice-bed interface where water pressure modulates the rate of ice sliding on a range of spatial and temporal scales (*1*–*3*). Water may also infiltrate into permeable beds and exert important controls on the deformability of the sedimentary subglacial substrate (*4*). The layer of actively deforming sediment near the interface with the ice sheet bottom (i.e., till) controls the speeds of ice streams, important corridors of rapid ice flow which drain ice sheets (*5*). Where subglacial water is discharged into the ocean, it entrains heat toward the ice-ocean interface and can drive substantial melting (*6*). Recent observational and modeling studies indicate that large portions of the Antarctic (*7*) and Greenland (*8*, *9*) ice sheets are underlain by sedimentary basins tens to thousands of meters deep. Magnetotelluric and seismic measurements in Antarctica have revealed that these sedimentary basins can be saturated throughout their thickness with water deriving from subglacial melting and fossil seawater (*10*). Although subglacial sediments host the largest water reservoir in continental Antarctica, there is no simple existing theory explaining the controls on the rates of water flow within these sediments and exchange between the sediment and subglacial drainage systems.

Observations have shown that in a wide range of aquifer environments, a decreasing load is supported by lower water pressure within the pore space of till, causing the sediment to contract (i.e., grains get closer together) (*11*–*13*). This phenomenon of sediment contraction forces water out through the upper boundary of the aquifer in a process known as exfiltration. In formerly glaciated regions, such as North America and Europe, the unloading of subglacial water-laden sediment during deglaciation continues to drive exfiltration even millennia after the end of the last ice age (*14*). The exfiltration and infiltration driven by past glaciations have been studied using hydromechanical numerical models (*15*–*17*). Other hydromechanical modeling studies have considered an idealized, Antarctic-like retreating ice sheet margin and found that high rates of retreat could lead to exfiltration rates of up to 20 mm/a over time scales of hundreds to thousands of years (*7*). However, on the decadal time scale associated with contemporary rates of observed ice sheet thinning (*18*), we lack estimates for potential rates of exfiltration. A simple expression for subglacial exfiltration rate would not require running a complex mechanical model for sediment deformation and fluid flow, enabling the quantification of exfiltration rates and their dependence on a broad range of uncertain parameters governing the hydromechanical properties of subglacial sediment.

Here, we develop a theory for the movement of water within, into, and out of subglacial sediment due to changes in thickness of overlying ice sheets. We show that the analytical expressions from this theory match numerical simulations from a more complex and computationally expensive hydromechanical model. We also use this theory to make a prediction for exfiltration rates driven by recent Antarctic Ice Sheet thinning. We find that, under certain conditions, exfiltration of water from subglacial sediment may dominate the subglacial water budget in rapidly thinning regions of West Antarctica. We conclude with a discussion of the implications of potentially large exfiltration fluxes from ice sheets and the prospect for including groundwater interactions in models of subglacial hydrology.

RESULTS AND DISCUSSION

Hydromechanical model and theory for subglacial exfiltration rate

We consider the flow of water through a porous sedimentary half-space overlain by a layer of glacier ice (*13*), as illustrated in Fig. 1. One-dimensional (positive down along z) fluid flow through a

[1]School of Earth and Atmospheric Sciences, Georgia Institute of Technology, 311 Ferst Drive, Atlanta, GA 30318, USA. [2]Thayer School of Engineering, Dartmouth College, Hanover, NH 03755, USA. [3]Hydrologic Science and Engineering Program, Department of Geophysics, Colorado School of Mines, Golden, CO 80401, USA. [4]U.S. Geological Survey, Geology, Geophysics, and Geochemistry Science Center, Lakewood, CO 80225, USA.
*Corresponding author. Email: robel@eas.gatech.edu

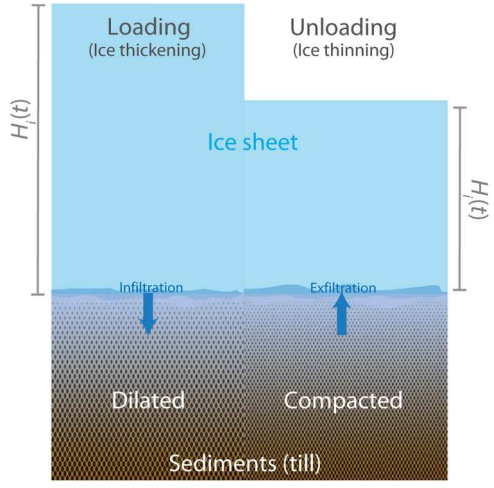

Fig. 1. Illustration of exfiltration and infiltration processes. Illustration explains how exfiltration or infiltration of groundwater occurs due to unloading or loading of ice sheets over saturated subglacial sediment half-space. At the ice-sediment interface, $z = 0$ and z increases down into sediment.

porous medium that is mechanically loaded can be described by Darcy flow with a source term (referred to hereafter as the "hydromechanical model")

$$S\frac{\partial h}{\partial t} = \frac{k\rho_w g}{\mu_w}\frac{\partial^2 h}{\partial z^2} + \frac{S\xi\rho_i}{\rho_w}\frac{\partial H_i}{\partial t} \quad (1)$$

where h is the hydraulic pressure head within the sediment (m), S is the sediment specific storage capacity (m^{-1}), k is the sediment permeability (m^2), ρ_w is the density of water, ρ_i is the density of glacier ice (kg/m^3), g is the acceleration due to gravity (m/s^2), μ_w is the viscosity of water (Pa·s), ξ is the dimensionless loading efficiency (also known as Skempton's constant, describing the fraction of the mechanical loading that causes pressure change with the sediment pore fluid), and $H_i(t)$ is the time-dependent thickness of overlying glacier ice (m). In the following discussion, we always assume that the hydraulic pressure head within the sediment begins at a steady-state ($\partial h/\partial t = 0$ at $t = 0$), and there are two boundary conditions

$$\frac{\partial h}{\partial z} = 0 \text{ as } z \to \infty \quad (2)$$

indicating no water flux into or out of the sediment at depth, and

$$h = \frac{\rho_i}{\rho_w} H_i(t) \text{ at } z = 0 \quad (3)$$

indicating pore pressure at the sediment surface balances the weight of overlying ice (i.e., zero effective pressure in voids at the sediment surface), consistent with the loading term (second term on right-hand side) in Eq. 1. This model as presented makes several assumptions: (1) The sediment is saturated with water, (2) the sediment is vertically extensive, and (3) horizontal mechanical strains are negligible compared to vertical strains. Assumption (1) precludes any more complex behavior arising from water flow into voids within the pore space that would not be described accurately by Darcy flow. Assumption (2) leads to the form of the lower boundary condition (Eq. 2) and can be replaced with an assumption of finite sediment thickness, but this would then require a numerical solution to the hydromechanical model which would no longer be analytically solvable. Assumption (3) permits us to neglect horizontal gradient terms that arise in the full three-dimensional version of Eq. 1 (*14*). Recent studies (*7*, *10*, *19*) indicate that assumptions (1) and (2) hold over extensive regions under the Antarctic Ice Sheet. Assumption (3) holds well in places where the ice loading rate and bed elevation do not change substantially over horizontal length scales of kilometers (*14*). In Antarctica, this final assumption generally holds more than a few kilometers upstream of the grounding line or terminus, where horizontal strains within the sediment due to variations in ice sheet thinning rate are likely small compared to vertical strains. Within kilometers of the grounding line or terminus, a two- or three-dimensional version of the hydromechanical model would be necessary to determine the complex flow pathways of groundwater (*14*, *15*). However, in this study, we will not consider exfiltration rates within less than 5 km of the grounding line, thus ensuring that this assumption remains valid.

To derive a closed-form expression for the exfiltration rate due to changes in ice sheet thickness from the above model, we consider two simple cases for the change in ice sheet thickness. In both cases, we use a Laplace transform to derive closed-form solutions for the evolution of hydraulic pressure head at all z and t, although here, we only discuss the behavior of the solution at the sediment surface. This method of solving the diffusion equation in various forms has substantial precedence and has been applied to flow through porous media going back to early work by Terzaghi (*20*) and Gibson (*21*). To our knowledge, there is no closed-form solution for the exfiltration rate available in the literature on subglacial sediment aquifers (with their particular boundary conditions), although we note that Lemieux *et al.* (*22*) has considered a related problem without closed-form solutions for exfiltration rate. Here, we focus on boundary conditions specific to subglacial sediment and the groundwater flux at its upper surface. In the first case, we assume constant rate of ice thickness change over time (i.e., $\partial H_i/\partial t$ is constant) and derive (see Materials and Methods) a simple closed-form solution for the time-dependent groundwater flux [$q = (k\rho_w g/\mu_w)\partial h/\partial z$] out of the surface of the sediment

$$q_c = -2(1-\xi)\frac{\partial H_i}{\partial t}\left(\frac{t}{\tau}\right)^{1/2} \quad (4)$$

where the subscript "c" denotes "constant" loading rate, and

$$\tau = \frac{\pi\rho_w\mu_w}{k\rho_i^2 gS} \quad (5)$$

is the diffusion time scale of water in the sediment. Positive q_c indicates an exfiltration flux out of the sediment and correspondingly, negative q_c is an infiltration flux into the sediment.

Similarly, we also consider the case of a step change in ice thickness of magnitude ΔH at time $t = 0$, such that the rate of change of ice thickness is the Dirac delta function. In this case, we also derive (see Materials and Methods) a closed-form solution for the time-dependent groundwater flux out of the surface of the sediment

$$q_d = -(1-\xi)\Delta H\left(\frac{1}{\tau t}\right)^{1/2} \quad (6)$$

where the subscript "d" denotes a "delta" loading rate.

The derivations of these closed-form expressions for groundwater flux at the sediment surface are exact solutions, requiring no

additional assumptions or approximations, beyond those made in the formulation of the hydromechanical model (Eqs. 1 to 3). Thus, a numerical solution of the hydromechanical model [including those implemented in prior studies of subglacial exfiltration (*7*, *15*, *23*)] should itself approximate these exact solutions. We demonstrate this correspondence in Fig. 2, which plots a numerical solution to the hydromechanical model for a case where the exfiltration flux is driven by 20 years of ice thinning at 5 m/a, followed by no thinning (see Materials and Methods for numerical details). This case is representative of the magnitudes and time scales of ice sheet thinning observed over West Antarctica and parts of Greenland in recent decades (*18*). During the period of ice thinning, the expression for groundwater flux driven by a constant ice thinning rate (blue line, q_c from Eq. 4) closely matches the numerical solution (black crosses). Following the cessation of ice thinning ($\partial H_i/\partial t = 0$ m/a), the slow reduction in exfiltration rates generally follows the theory for a step change in ice thickness (red line, q_d from Eq. 6, where the onset time is set to $t = 10$ years, i.e., the midpoint of thinning). Because the duration of ice thinning in this case is fast compared to the diffusion time scale of water in sediment (τ), the sediment response following the cessation of this short period of ice thinning is similar to the response to a step change in ice thickness (in this case, with $\Delta H = 100$ m), and so the analytical solution matches the numerical solution closely during this period as well.

There are several important aspects of the time-evolving rate of exfiltration captured in Eqs. 4 and 6. First, the exfiltration rate is linearly proportional to the rate (dH_i/dt) or magnitude (ΔH) of ice thinning. Thus, the exfiltration rates that could be expected from modern rates of ice sheet thinning (m/a) should generally be one to two orders of magnitude higher than those previously simulated in response to ice sheet thinning during the last deglaciation [tens of cm/a; (*15*, *23*)]. Second, the same change in ice thickness, applied over a shorter duration, leads to higher peak exfiltration rates (proportional to $\Delta t^{-\frac{1}{2}}$ where Δt is the duration of ice thickness change). Third, although there is initially a rapid reduction in exfiltration rates after ice thinning stops (proportional to $t^{-\frac{1}{2}}$, where t is the time since the end of thinning), exfiltration rates will remain elevated for a long time period (Fig. 2) as water continues to flow up from deep in the subglacial aquifer. Last, the rate of increase in exfiltration rate in response to ice thinning is fundamentally set by τ, the diffusion time scale of water in the sediment. Through τ, we expect that the exfiltration rate depends on $(1-\xi)(kS)^{\frac{1}{2}}$, with loading efficiency (ξ), permeability (k), and specific storage capacity (S), being the principal parameters describing the mechanical properties of sediment. That is, ξ describes the extent of sediment pore pressure change in response to the load change, k describes the ease of water flow through sediment pores, and S describes the extent of sediment water content change due to a change in pore pressure. Thus, two orders of magnitude difference in sediment permeability or specific storage leads to one order of magnitude difference in exfiltration rate at the same time after the onset of thinning. For a given τ, continued thinning will drive increasing exfiltration rates as the square root of time since thinning onset ($t^{\frac{1}{2}}$).

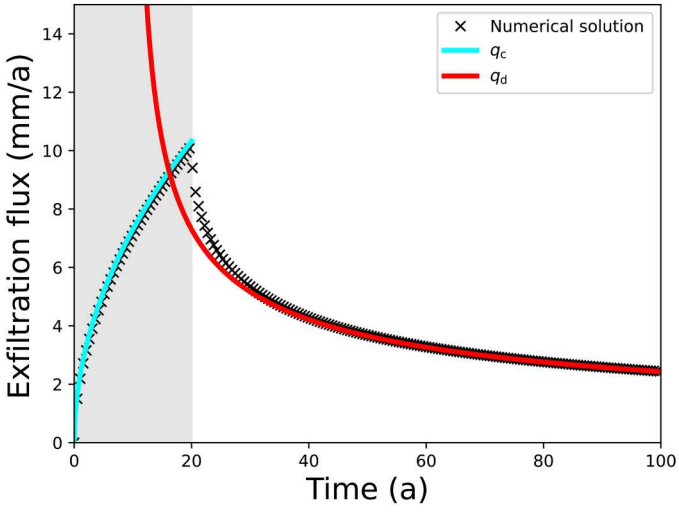

Fig. 2. Exfiltration rate evolution in response to a constant ice sheet thinning rate, stopping after 20 years. Exfiltration rate as a function of time simulated numerically in the hydromechanical model (black crosses; Eqs. 1 to 3). Solid lines show the exfiltration predicted by a closed form theory when ice thinning rate is constant (q_c, blue solid line) and for a step change in ice sheet thickness (q_d, red line). This simulation assumes that $k = 10^{-15}$ m^2, $S = 10^{-6}$ m^{-1}, $\xi = 0.2$, $\rho_i = 920$ kg/m^3, $\rho_w = 1000$ kg/m^3, $\mu_w = 10^{-3}$ Pa·s, $g = 9.81$ m/s^2, and $\partial H_i/\partial t = 5$ m/a for the first 20 years of the simulation (gray shaded region). Numerical details are discussed in Materials and Methods.

Predicted exfiltration rate due to contemporary Antarctic Ice Sheet thinning

Rapid thinning near the margins of the Antarctic Ice Sheet has been well documented by satellite observations over the past several decades (*24*). Since 2003, NASA's Ice, Cloud, and land Elevation Satellite missions (ICESat and ICESat-2) have provided measurements of ice sheet elevation at high spatial and temporal resolution around Antarctica. With these measurements, Smith *et al.* (*18*) derived accurate and extensive maps of the mean Antarctic Ice Sheet thinning rate (dH_i/dt) from 2003 to 2019 at 5 km resolution. The simplicity of Eq. 4 allows us to make predictions for the exfiltration rate at the end of this 16-year period driven by the measured ice sheet thinning rate (Fig. 3). Other than the thinning rate, the only other inputs required to make this prediction are the physical parameters in Eq. 4. We consider a representative set of permeabilities spanning the range of estimates for Antarctic subglacial sediments (*25*–*27*) and otherwise assume the parameter values given in caption of Fig. 3. The assumption that horizontal variations in loading rate are negligible over length scales of a few kilometers, which goes into the hydromechanical model (Eq. 1), is generally valid for the following prediction, since the thinning rate product of Smith *et al.* (*18*): (1) is too coarse (at 5 km resolution) to resolve such small-scale variations and (2) is smooth over horizontal length scales of tens to hundreds of kilometers.

For a high but realistic permeability ($k = 10^{-13}$ m^2), Fig. 3A shows that in regions of rapid ice sheet thinning in the Amundsen Sea Embayment and Wilkes Land, predicted rates of exfiltration span, and in some places exceed, 10 to 100 mm/a. These potentially rapid rates of exfiltration extend hundreds of kilometers upstream into the catchments of ice streams, where dynamic thinning occurs. In this case, the total predicted water flux over all of Antarctica due solely to exfiltration is 6.9 Gt/a, with 4.3 Gt/a of that total from West Antarctica, and 2.8 Gt/a over Thwaites and Pine Island glaciers. In other areas of thickening (i.e., Kamb Ice Stream and Queen Maud Land), we predict infiltration rates of 1 to 10 mm/a. These predicted

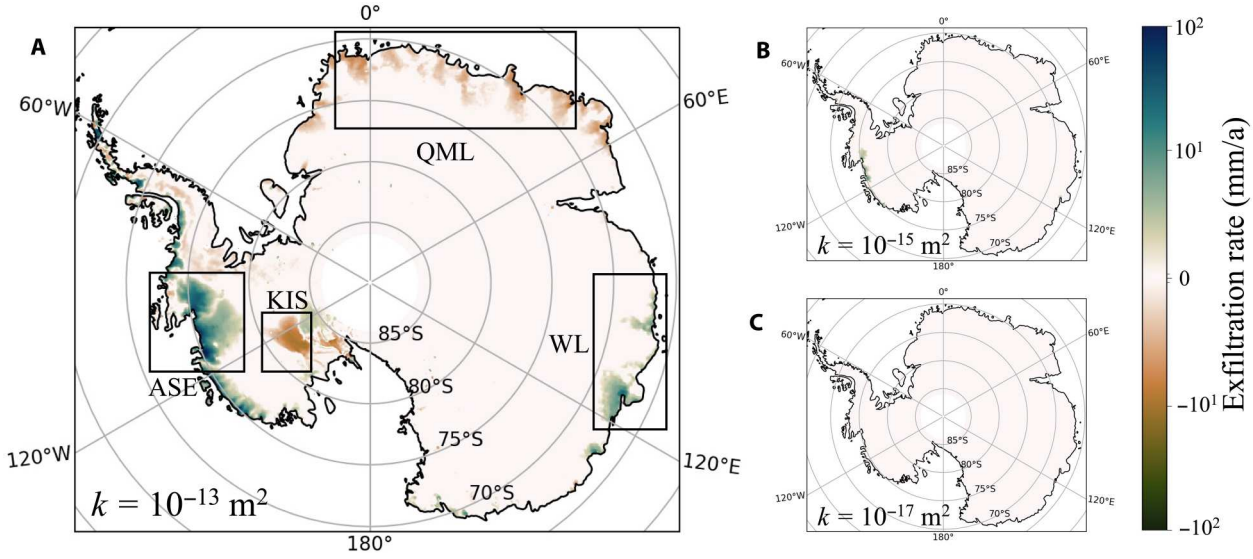

Fig. 3. Predicted contemporary exfiltration rates under the Antarctic Ice Sheet for different sediment permeabilities. Map of predicted exfiltration rate due to ice sheet thinning estimated by ICESat and ICESat-2 from 2003 to 2019, assuming sediment permeabilities of (**A**) $k = 10^{-13}$ m^2, (**B**) $k = 10^{-15}$ m^2, and (**C**) $k = 10^{-17}$ m^2. These predictions assume $S = 10^{-6}$ m^{-1}, $\xi = 0.2$, $\rho_i = 920$ kg/m^3, $\rho_w = 1000$ kg/m^3, $\mu_w = 10^{-3}$ Pa·s, and $g = 9.81$ m/s^2. Negative values in all panels indicate infiltration due to ice sheet thickening. In (A), regions discussed in text are labeled: ASE, Amundsen Sea Embayment; WL, Wilkes Land; KIS, Kamb Ice Stream; QML, Queen Maud Land.

exfiltration and infiltration rates (Eq. 4) depend on the permeability such that $q \sim k^{\frac{1}{2}}$, which explains the decrease in predicted exfiltration rate by an order of magnitude in Fig. 3B where $k = 10^{-15}$ m^2 and two orders of magnitude in Fig. 3C where $k = 10^{-17}$ m^2.

To put these predictions into context, we consider how exfiltration of water out of sediment adds to the water produced by basal ice melt at the ice-sediment interface. Figure 4 plots the total fraction of the local basal water budget that would be occupied by the predicted exfiltration rates $[q_c/(q_c + q_m)$, where q_m is the basal melt rate] using an estimate of basal melt rate from Pattyn *et al.* (*28*). We find that for high, but realistic permeability, predicted exfiltration would account for a substantial fraction (i.e., more than half) of the local basal water budget at the ice-sediment interface in regions of rapid ice sheet thinning (Fig. 4A). In general, exfiltration is the dominant contributor to the basal water budget tens to hundreds of kilometers upstream of the grounding line of rapidly thinning glaciers, where thinning is high, but frictional heat production at the bed is low (due to slower ice sliding speeds). In many places (dark green in Fig. 4A) where there is some thinning, but no predicted basal ice melting, water exfiltration from subglacial sediment is predicted

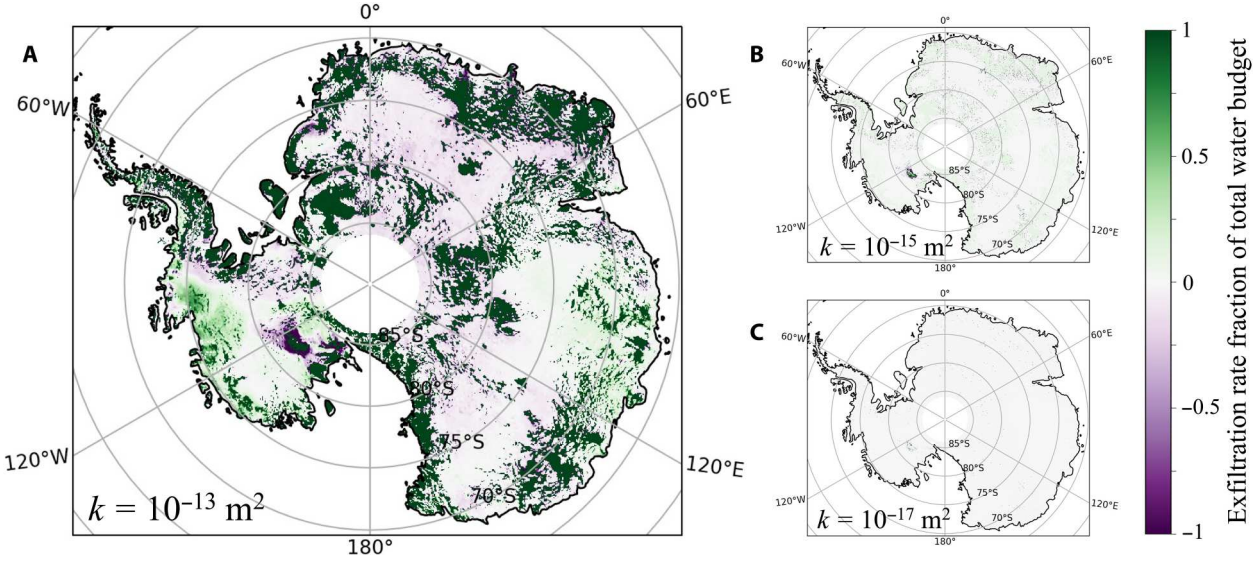

Fig. 4. Predicted fraction of local basal water budget due to exfiltration or infiltration. Map of predicted fraction of local basal water budget due to exfiltration or infiltration, using predictions from Fig. 3 using ice-sheet-wide basal melt rate estimate from Pattyn *et al.* (*28*). As in Fig. 3, panels correspond to different permeability values: (**A**) $k = 10^{-13}$ m^2, (**B**) $k = 10^{-15}$ m^2, and (**C**) $k = 10^{-17}$ m^2. Negative values in all panels indicate infiltration due to ice sheet thickening.

to be the only source of water at the ice-sediment interface. However, these are also likely to be regions where subglacial sediment includes frozen fringes near the ice-sediment interface which may prevent exfiltration from occurring. A more complex thermomechanical sediment model would be necessary to understand the fate of groundwater in these regions. For our high permeability case, the predicted exfiltration accounts for 10% of the total Antarctic basal water budget, 21% of the West Antarctic basal water budget, and 38% of the Thwaites and Pine Island basal water budget. Assuming that all basal water drains to the ocean, this prediction would nearly double the total subglacial water discharge into the Amundsen Sea compared to estimates based on basal melting alone. This calculation does not account for potential horizontal redistribution of water along the ice-sediment interface but does highlight that rapid thinning may be introducing large water volumes to this interface in regions with relatively little local basal melting.

Thinning rates during the ICESat satellite missions were not uniform in time, and have been accelerating in regions such as the Amundsen Sea Embayment since the early 1990s (*29*). A numerical simulation (not plotted here) indicates that including a steady acceleration in thinning rates (with the same mean measured thinning rate) over 2003 to 2019 would increase contemporary exfiltration rates by another 30%. In addition, thinning in the decades before the availability of ICESat data (*30*, *31*) and even earlier in the Holocene (*32*–*34*) may drive exfiltration rates even higher than estimates here, although the uncertainty on thinning rates increases substantially before the satellite laser altimetry records that we focus on here. In the future, Antarctic Ice Sheet thinning is expected to continue at current rates or increase further (*35*). For continued ice sheet thinning at the same rates as today, our theory suggests that by 2100 exfiltration rates will grow by another 250% due to the square root dependence on duration of thinning in Eq. 4. For even higher thinning rates (predicted by most credible models of future Antarctic Ice Sheet change), exfiltration rates in 2100 would likely be more than four times what they are today.

Exfiltration-driven changes to sediment void ratio

Flux of water into or out of sediment is a potentially important contributor to the subglacial water drainage system that exists at the ice-sediment interface. However, it may also change the sediment water content, which partly controls the plastic yield stress of the uppermost till layer and the rate at which it deforms (*5*). We can estimate the rate at which the void ratio (i.e., the ratio of water-filled void volume to solid volume in a porous medium) at the sediment surface changes in response to ice sheet thinning, by using the solution to the hydromechanical model under a constant thinning rate to calculate the flux divergence of water at the sediment surface

$$\left.\frac{\partial q}{\partial z}\right|_{z=0} = (1-\xi)S\frac{\rho_i}{\rho_w}\frac{\partial H_i}{\partial t} \tag{7}$$

Christoffersen *et al.* (*36*) estimated the contemporary water flux into and out of subglacial sediment in the Siple Coast region of West Antarctica, where ice streams exhibit dynamic fluctuations in velocity on multicentennial time scales (*37*). To do so, they calculated the water flux at the ice-sediment interface necessary to explain the change in void ratio over a thin layer of deforming till consistent with observed changes in ice stream velocity from 1997 to 2009. At the slowing Whillans Ice Stream (*38*, *39*), they calculated a spatially averaged void ratio change rate of 6×10^{-4} a^{-1}, which corresponds to an exfiltration rate of approximately 6 mm/a. Given observed thinning rates of 0.5 − 1 m/a over upper Whillans Ice Stream during the latter half of the 20th century (*40*–*42*) and specific storage (S) of 10^{-4} to 10^{-3} m^{-1}, we estimate a void ratio change rate of 10^{-5} to 10^{-3} a^{-1}, which is consistent with the change rate estimated by Christoffersen *et al.* (*36*). Averaging the void ratio change only over the portions of upper Whillans Ice Stream that are actually thinning produces an even lower estimate of void ratio change rate [10^{-4} a^{-1}; based on figure 3B in Christoffersen *et al.* (*36*)], which is consistent with values of sediment specific storage (S) of 10^{-5} to 10^{-4} m^{-1}, which have been observed at glaciers outside of Antarctica (see discussion in next section). The estimated exfiltration rates are also consistent with exfiltration rates that are predicted by Eq. 4, given a sediment permeability in the range of 10^{-15} to 10^{-13}. Such agreement between our theory and Christoffersen *et al.* (*36*) results suggests the possibility that exfiltration (or infiltration at the thickening Kamb Ice Stream) plays an important role in the stagnation-activation cycle of ice streams.

Other considerations such as the heat flux at the ice-sediment interface may have an important impact on the void ratio and yield stress of sediment through changes to the melt rate of basal ice. As Gooch *et al.* (*23*) found, heat is advected by groundwater exfiltration toward basal ice, suggesting a potential role for exfiltration and infiltration in centennial-scale ice stream flow variability. Prior theories for stagnation-activation cycles of ice streams (*43*–*45*) mainly assume that subglacial meltwater can enter or leave sediment purely based on consideration of thermodynamics and water availability. Although exfiltration and infiltration due to load changes are not necessary to explain variability in ice stream velocity, these results do indicate that considerations of pressure change at the ice-sediment interface may play an important role in such variability. To assess the importance of these complex interactions will require coupled models of hydrology and thermodynamics in sediment, subglacial drainage, and basal ice.

Uncertainties in predicted exfiltration rates

The largest uncertainty in the predicted exfiltration rates of this study is the permeability of subglacial sediment. Direct laboratory measurements of sediment recovered from beneath glaciers in Antarctica and elsewhere indicate a wide range of 10^{-17} to 10^{-13} m^2 (*26*, *27*, *46*). Indirect methods that are more likely to account for the extreme mechanical conditions existing for sediments in situ have generally produced higher estimates of the permeability of sediments up to 10^{-10} m^2 (*25*, *47*, *48*). High-fidelity numerical simulations also indicate that sheared subglacial sediments exhibit a permeability increase of one to two orders of magnitude in the upper centimeters of the deforming till layer (*49*, *50*), which could initially yield higher exfiltration rates immediately after the onset of unloading, followed by a less rapid increase in exfiltration rates as water flows from below the deforming till layer. In laboratory experiments, subglacial sediment collected from the Siple Coast has been observed to produce substantial increases in permeability when unloaded (*27*), which would further increase the exfiltration rate. If permeability were at the absolute lower end of the range in the literature (i.e., more consistent with impermeable basement rock or high-clay sediments), exfiltration rates would be negligible. By the same token, indirect in situ estimates of Antarctic sediment

permeability from a model (*48*) support even higher exfiltration rates than plotted in Fig. 3A. The potential importance of the exfiltration rates predicted here indicates the need for better constraints on the effective permeability of sediments in their natural state beneath fast-flowing glaciers (*25*).

Specific storage (S) is also poorly known, with estimates under glaciers or in formerly glaciated landscapes varying between 10^{-7} to 10^{-4} m^{-1} (although no known estimates for Antarctic subglacial sediment) (*51*, *52*). Again following prior studies of subglacial exfiltration, we take $S = 10^{-6}$ m^{-1} (*22*, *23*) for the predictions in Figs. 3 and 4, although noting this is a conservatively low value of specific storage. Taking values closer to those inferred for Trapridge Glacier in Canada, one of the only estimates of S directly from an existing and thick subglacial sediment glacier (*51*) would yield exfiltration rates one order of magnitude higher than predicted here, due to the dependence of exfiltration rates on $S^{\frac{1}{2}}$ in our closed-form theory (Eq. 5). Similarly, we can see that a moderate permeability ($k = 10^{-15}$ m^2) with high but realistic specific storage ($S = 10^{-4}$ m^{-1}) would yield the same predicted exfiltration rates as in Fig. 3A.

Loading efficiency (ξ) has not been measured for Antarctic sediments, so here, we assume a value of 0.2, as in prior modeling studies of exfiltration (*22*, *23*). Although such a loading efficiency is at the bottom of the range of values measured for glacial sediments in North America (*52*), the uncertainty introduced into predicted exfiltration rates from loading efficiency is small compared to the uncertainties in permeability and specific storage.

The extent of subglacial sedimentary basins has not been constrained well by geophysical observations. Li *et al.* (*7*) attempt to remedy this through the use of machine learning methods to classify the likelihood of subglacial sedimentary basins over all of Antarctica using extensively observed quantities (e.g., bed topography and magnetic and gravity data) as predictors. In fig. S1, we overlay this sedimentary basin likelihood map on our exfiltration prediction and find that it is still highly uncertain whether sedimentary basins exist beneath almost all regions predicted to be experiencing substantial exfiltration (i.e., probability between 33 and 66%). Put another away, in these regions, the presence of subglacial sediment can neither be definitely ruled in or out with high confidence. This underscores the need for better geophysical constraints on the extent of subglacial sedimentary layers in the regions we find may potentially be experiencing high rates of exfiltration.

The role of basal ice melting in the subglacial water budget is also uncertain due to a lack of direct constraints and intermodel differences. Estimates of geothermal heat flux under Antarctica vary substantially between different Earth models (*53*). Prior studies (*7*, *23*) have also suggested that exfiltration of water may itself advect heat from deeper within the warm subglacial sediment layer, which can increase the effective geothermal heat flux at the upper sediment surface. Such estimates of heat advection by groundwater flow are sensitively dependent on the treatment of water once it leaves the sediment layer, which sets the thermal boundary condition at the sediment surface. Notwithstanding such possibilities, typical uncertainties in geothermal heat flux (*53*) amount to 1 to 10 mm/a of uncertainty in basal melt rates, whereas uncertainty in the rate of frictional heating under fast-flowing ice streams greatly exceeds that, largely related to how basal friction is estimated (*28*, *54*, *55*). In fig. S2, we find the results plotted in Fig. 4A to be qualitatively consistent across several other model-based estimates of Antarctic basal melt rates (with some disagreement about which areas of the bed are frozen). Although some other models do predict higher basal melt rates than Pattyn *et al.* (*28*), there is a limit on the highest basal melt rates achievable because the fastest sliding areas of the Antarctic Ice Sheet are also the areas with the lowest friction.

Measurements of exfiltration under and near ice sheets

Subglacial groundwater exfiltration driven by ice sheet thinning has yet to be directly measured by conventional hydrogeological techniques. However, recent studies have made other relevant measurements that are indicative of subglacial groundwater discharge. Using seepage meters at the seafloor, Uemura *et al.* (*56*) directly measured high rates (3 to 30 m/a) of submarine groundwater discharge at several sites within kilometers of the current ice sheet margin in East Antarctica. One possible explanation for this groundwater discharge is the recent retreat of the ice sheet from these areas of the seafloor causing a near-instantaneous unloading and potentially rapid exfiltration persisting over long time scales. In addition, Liljedahl *et al.* (*57*) reported direct measurements of hydraulic head within a deep borehole angled beneath a land-terminating portion of the western margin of the Greenland Ice Sheet. Over seven years of measurements, they found steadily decreasing hydraulic head across 300 m of a deep fractured bedrock aquifer at a rate that is consistent with the rate of ice sheet thinning at this margin, suggestive of mechanical unloading that is nearly uniform over the aquifer column. All of these measurements agree with our prediction of a potentially important role for subglacial groundwater exfiltration driven by ice sheet thinning. In the future, measuring the horizontal extent of subglacial aquifers using electromagnetic and hydrogeological techniques would yield important constraints on the potentially important role of exfiltrated water in the subglacial water budget. Miniaturization of typical hydrogeological sensors would be required to be able to gain access to the ice sheet base through a borehole.

High rates of exfiltration may also represent a source of water with considerably different chemistry than basal meltwater (*10*, *58*). If subglacial discharge to the ocean is much more enriched in minerals from groundwater than previously recognized, there could be substantial implications for subglacial biogeochemical processes (*34*, *59*) and nutrient delivery to marine ecosystems (*60*, *61*). Field measurements constraining the contribution of exfiltration to subglacial discharge would be important inputs to estimates of the nutrient fluxes to the ocean, with implications for understanding marine biological communities in polar oceans.

Potential feedbacks of subglacial exfiltration on ice sheet evolution

Our predictions for exfiltration rate indicate that, for either high sediment permeabilities or high specific storage, the total exfiltration water flux may be an important contributor to subglacial discharge to the ocean. In the fastest thinning parts of Antarctica, in particular the Amundsen Sea Sector, including exfiltration in the subglacial water budget could double the rate of subglacial discharge to grounding lines of already rapidly retreating glaciers. One potential influence of this higher subglacial water discharge would be feedbacks on the rate of melt at the ice-ocean interface. In numerical model parameterizations, the dependence of the melt rate at the ice-ocean interface on subglacial discharge rate ranges from sublinear (exponent of 0.39) at vertical ice fronts (*62*) to approximately linear at floating ice shelves (assuming free-stream velocity is set by

subglacial discharge rate) (*63*). Thus, a doubling of subglacial discharge rate would lead to anywhere from 30% (sublinear dependence) to 100% (linear dependence) higher melt rates under floating ice and constitute a positive feedback on dynamic thinning of ice sheets. This previously unrecognized source of subglacial water discharge may be the reason why models tend to underpredict contemporary sub-ice shelf melt rates at Pine Island Glacier ice shelf (*64*) and Getz Ice Shelf (*6*), both of which have catchments that we predict to have potentially high rates of exfiltration (Fig. 3A). Thus, including exfiltration into models of subglacial hydrology and ice sheet evolution could improve model correspondence to observations of ice melt at the ice-ocean interface.

The transport of heat to subtemperate or frozen regions of the bed by exfiltrated water could play a role in accelerating ice flow in upstream regions of ice streams (*65*), extending the reach of dynamic thinning (*66*–*68*). However, the extent of such a response depends on whether ice sliding is accommodated by sediment deformation, subglacial drainage, or some combination of the two. As discussed previously, thinning ice drives exfiltration, which reduces the water content of the uppermost actively deforming "till" layer. Previous experimental studies of the yield stress of subglacial till in Antarctica (*5*) indicate that a decrease in till void ratio of 0.01 would increase basal yield (and shear) stress by ~20%. Thus, for ice thinning at 1 to 10 m/a over multidecadal time scales, exfiltration could act as a nonnegligible (i.e., more than a few %) negative feedback on ice flow by till deformation if specific storage (S) is at the high end of previously measured values for subglacial sediments (10^{-5} to 10^{-4} m^{-1}). In addition, if the sediment layer is thin, then groundwater exfiltrated out of the sediment is not replaced by groundwater flow from deep, potentially leading to even more rapid decrease in the water content of the actively deforming till layer. This may be an avenue by which exfiltration drives a negative feedback on ice flow speed.

Groundwater leaving subglacial sediment enters the subglacial drainage system. The form of drainage existing at subglacial ice-sediment interfaces is not well understood because observations are sparse (*69*) and models of subglacial hydrology disagree on the erodibility of sediment compared to ice (*70*–*73*). Models have been proposed for subglacial drainage through canals incised downward into sediment in which ice sliding speed increases with subglacial water discharge (*74*). Conversely, models of subglacial drainage through channels incised upward into ice generally find that ice sliding speed decreases with increasing subglacial water discharge over long time scales (*2*). Among the latter type of models, wide variation also exists in model formulation, and so sensitivity of basal water pressure to a given increase in water supply to the ice-bed interface varies by more than an order of magnitude across models (*75*). Thus, it is difficult to predict how the consideration of exfiltration would change ice sliding or even the sign of such a change. In addition, calculating the effect of the extra subglacial water supply from exfiltration on ice sliding at the ice sheet scale is not currently possible in coupled models of subglacial hydrology and ice sheet evolution due to the computationally intensive nature of existing numerical models of subglacial hydrology, although progress is being made on this problem (*76*). However, even just the potential for large changes in subshelf melt rates, basal shear stress, and ice sliding from additional subglacial discharge argues for the inclusion of groundwater into numerical ice sheet models.

Subglacial exfiltration and infiltration are responses to changes in the effective pressure at the ice-sediment interface, which is the difference between ice overburden pressure and local water pressure. The theory developed thus far has focused on how changes in ice overburden pressure can drive exfiltration particularly in places, like Antarctica, where variations in subglacial water pressure are not substantial on short times scales. The potentially higher rates of subglacial discharge discussed above would occur throughout the entire year in Antarctica. Conversely, in glaciers with substantial surface melt (i.e., Greenlandic or mountain glaciers), exfiltration is unlikely to be a substantial contributor to the subglacial water budget at the peak of the melt season. However, at glaciers experiencing seasonal or diurnal variability in meltwater supply to the bed, subglacial channels may experience rapid depressurization over hours to weeks as the melt season comes to an end [as in other hydrological systems experiencing variability (*77*–*79*)]. Since the peak exfiltration flux is proportional to the rate of unloading (Eq. 4), rapid variability in pressure head at the sediment surface is capable of driving exfiltration at rates that approach the supply of meltwater during the melt season (fig. S3), sustaining some form of drainage over winter months. This may explain the puzzling persistence of subglacial drainage systems during the winter at some glaciers, which has previously been attributed to englacial water storage (*80*, *81*). Liljedahl *et al.* (*57*) find such diurnal- to seasonal-scale variations in hydraulic head deep within a relatively impermeable fractured bedrock aquifer (which is unlikely to support direct water injection to such depths on short times scales), indicating that hydraulic loading drives deep pressure variations even on diurnal to seasonal time scales.

The potentially important role of exfiltration in supplying water to the ice-sediment interface should also motivate further work to incorporate the hydromechanical model of groundwater flow into numerical models of ice sheet and subglacial drainage coevolution. The ice sheet response to this source of subglacial water ultimately depends on the representation of subglacial drainage and sliding within ice sheet models. However, the results of this study show that groundwater-drainage interactions beneath an ice sheet may be important even on the short decadal scales that have been the focus of so much recent effort in ice sheet projections (*82*, *83*). Our results highlight the potential benefits of extending our conceptual and numerical models of ice sheet dynamics beyond the sediment interface.

MATERIALS AND METHODS

Theory of exfiltration from a porous half-space

Most of what follows is inspired by (*22*), although with some key differences. We ultimately come to different closed form solutions for the hydraulic pressure head as a function of time and space, which lead to closed-form solution for surface flux and flux divergence under two different loading scenarios.

We consider a one-dimensional column of subglacial sediment, below a column of glacier ice that is changing in thickness. We start with a simplified form of the diffusion equation applied to flow through a one-dimensional porous medium (i.e., derived from combining Darcy's law with mass conservation)

$$\frac{\partial h}{\partial t} = D\frac{\partial^2 h}{\partial z^2} + L \tag{8}$$

where h is the hydraulic pressure head within the porous medium, $D = \kappa/S$ is the hydraulic diffusivity, which depends on the hydraulic conductivity (κ) and specific storage (S), z is the vertical coordinate, and

$$L = \frac{\xi \rho_i}{\rho_w} \frac{\partial H_i}{\partial t} \tag{9}$$

is the rate at which the porous column is loaded or unloaded (in this case due to a change in overlying ice thickness) causing a change in sediment dilatancy, with ξ being the one-dimensional loading efficiency (also known as Skempton's constant, describing the fraction of the mechanical loading that causes pressure change with the sediment pore fluid), $\rho_{i,w}$, the densities of ice and water, and $\frac{\partial H_i}{\partial t}$ the instantaneous rate of thinning or thickening of the overlying ice column that is loading the sediment. We consider two boundary conditions, the first one far from the ice-sediment interface

$$\left.\frac{\partial h}{\partial z}\right|_{z\to\infty} = 0 \tag{10}$$

indicating no water flux into the sediment at depth. The second boundary condition is at the ice-sediment interface

$$h(z=0) = \frac{\rho_i}{\rho_w} H_i(t) \tag{11}$$

where $H_i(t)$ is some prescribed function for the evolution of the overlying ice thickness as a function of time, which should be consistent with Eq. 9. Below, we will consider two forms for this function to derive an analytical solution to the diffusion problem: (i) constant $\frac{\partial H_i}{\partial t}$ and (ii) dirac delta function for $\frac{\partial H_i}{\partial t}$.

Constant ice thinning rate

Here is where it is important to consider the form of q. We consider the case where $H_i(t) = h_0 + \frac{\partial H_i}{\partial t} t$ and $\frac{\partial H_i}{\partial t}$ is a constant in time (i.e., a constant rate of loading or unloading at the upper boundary condition), which makes q a constant in time as well.

We proceed by using the Laplace transform for the pressure head

$$\overline{h}(p) = \int_0^\infty \exp(-pt) h(z,t) dt \tag{12}$$

where p is a complex frequency parameter. Inserting the transform into Eq. 8 and moving all terms to one side yields

$$\frac{\partial^2 \overline{h}}{\partial z^2} - \frac{p\overline{h}}{D} + \frac{q}{Dp} = 0 \tag{13}$$

When L is a constant, Eq. 13 has the following solution

$$\overline{h} = A\exp[z(p/D)^{1/2}] + B\exp[-z(p/D)^{1/2}] + \frac{L}{p^2} \tag{14}$$

The constants A and B are determined by applying the boundary conditions. Applying the lower boundary condition (Eq. 2) requires that $A = 0$ for the first term to go to zero at the boundary. Applying the upper boundary condition (Eq. 3) requires that

$$\overline{h} = \frac{L}{\xi p^2} \tag{15}$$

Another way of interpreting this boundary condition is that the source term in the diffusion equation involves a uniaxial loading or unloading modulated by the loading efficiency of the porous material (ξ), whereas the pressure at the column surface is directly set by the overlying pressure loading. Thus, the two terms end up being the same except for a factor of $1/\xi$. Applying this upper boundary condition gives B and fully determines the Laplace-transformed solution

$$\overline{h} = \frac{q}{p^2}\left(\frac{1}{\xi} - 1\right)\exp[-z(p/D)^{1/2}] + \frac{L}{p^2} \tag{16}$$

We can determine the nontransformed solution corresponding to Eq. 16 above by superposing the individual inverse transformed terms from the table of transforms in appendix V in (*84*).

$$h(z,t) = L\left(\frac{1}{\xi} - 1\right) \times \left[\left(t + \frac{z^2}{2D}\right) erfc\left(\frac{z}{2(Dt)^{1/2}}\right) - z\left(\frac{t}{\pi D}\right)^{1/2} \exp\left(-\frac{z^2}{4Dt}\right) + \frac{t}{1/\xi - 1}\right] \tag{17}$$

From this analytic solution, we can calculate the Darcy flux ($\kappa \frac{\partial h}{\partial z}$) at the surface of the porous column ($z = 0$). Ultimately, the spatial derivative eliminates several of the terms in the above expression, leading to a relatively simple expression for this exfiltration/infiltration flux

$$q_c = \kappa \left.\frac{\partial h}{\partial z}\right|_{z=0} = 2(1-\xi)\frac{\rho_i}{\rho_w}\frac{\partial H_i}{\partial t}\left(\frac{\kappa S}{\pi} t\right)^{1/2} \tag{18}$$

where we have substituted the definitions of q and D back in to derive this final expression.

Step change in ice thickness

We also consider another case where ice thickness changes through a step function with magnitude ΔH at $t = 0$, which corresponds to a Dirac delta function on thickness rate of change: $\frac{\partial H_i}{\partial t} = \Delta H \delta(t)$. In this case

$$L = \alpha \delta(t) \tag{19}$$

where $\alpha = \frac{\xi \rho_i}{\rho_w} \Delta h$.

We proceed by inserting $\overline{h}$ defined in the same way as above to derive the following transformed version of the hydromechanical equation

$$\frac{\partial^2 \overline{h}}{\partial z^2} - \frac{\overline{h}}{D} + \frac{\alpha}{Dp} = 0 \tag{20}$$

This equation has the same general form of a solution as in the prior case considered, with only a difference in the final term

$$\overline{h} = A\exp[z(p/D)^{1/2}] + B\exp[-z(p/D)^{1/2}] + \frac{\alpha}{p} \tag{21}$$

Inserting the boundary conditions yields the complete transformed solution

$$\overline{h} = \frac{\alpha}{p}\left(\frac{1}{\xi} - 1\right)\exp[-z(p/D)^{1/2}] + \frac{\alpha}{p} \tag{22}$$

Last, we can determine the nontransformed solution corresponding to Eq. 22 above by superposing the individual inverse transformed terms from the table of transforms in appendix V in (*84*).

$$h(z,t) = \alpha\left(\frac{1}{\xi} - 1\right)\left[erfc\left(\frac{z}{2(Dt)^{1/2}}\right) + \frac{1}{1/\xi - 1}\right] \quad (23)$$

From this analytic solution, we can calculate the Darcy flux ($\kappa\frac{\partial h}{\partial z}$) at the surface of the porous column ($z = 0$). Ultimately, the spatial derivative eliminates several of the terms in the above expression, leading to a relatively simple expression for this exfiltration/infiltration flux

$$q_d = \kappa\frac{\partial h}{\partial z}\bigg|_{z=0} = (1-\xi)\frac{\rho_i}{\rho_w}\Delta H\left(\frac{\kappa S}{\pi t}\right)^{1/2} \quad (24)$$

where we have substituted the definitions of q and D back in to derive this final expression.

Numerical methods used to solve hydromechanical model

The hydromechanical model (Eq. 8) is a version of the well-known diffusion equation with a source. To solve this equation, we use the Crank-Nicolson method (*85*), a widely used second-order finite difference method, which is implicit in time. Although it is merely conditionally stable, we generally consider time steps that are numerically stable and provide highly accurate solutions, as evidenced by the correspondence of the numerical method to the exact solution to the diffusion equation derived through the Laplace transformation above.

The Crank-Nicolson method blends explicit and implicit finite difference time-stepping schemes (forward Euler and backward Euler) to produce second-order accuracy. For the hydromechanical model, the resulting discretization is

$$\frac{h_i^{k+1} - h_i^k}{\Delta t} = \frac{D}{2\Delta z^2}[(h_{i+1}^{k+1} - 2h_i^{k+1} + h_{i-1}^{k+1}) + (h_{i+1}^k - 2h_i^k + h_{i-1}^k)] + L_i^k \quad (25)$$

where i indices indicate grid points in the spatial domain and k indices time steps. Rearranging such that terms in the k time step are on the right hand side and terms in the $k + 1$ time step are on the left hand side, we have

$$-\frac{1}{2}C_D h_{i+1}^{k+1} + (1 + C_D)h_i^{k+1} - \frac{1}{2}C_D h_{i-1}^{k+1} = \frac{1}{2}C_D h_{i+1}^k + (1 - C_D)h_i^k + \frac{1}{2}C_D h_{i-1}^k + L_i^k \quad (26)$$

where $C_D = \frac{D\Delta t}{\Delta z^2}$.

We have implemented this Crank-Nicolson method using sparse matrices and numpy array capabilities in a Jupyter notebook. Many previously published studies numerically solve the hydromechanical model here using closed-source software (*7*, *15*, *23*). Our goal here was to provide a straightforward and simple numerical solver for this method that can be widely used within the community to understand exfiltration better. This notebook is available through an open-source repository and as a Binder notebook that can be run on any modern internet browser without installing any software (see code availability).

Supplementary Materials

This PDF file includes:

Figs. S1 to S3

REFERENCES AND NOTES

1. G. K. Clarke, Subglacial processes. *Annu. Rev. Earth Planet. Sci.* **33**, 247–276 (2005).
2. C. Schoof, Ice-sheet acceleration driven by melt supply variability. *Nature* **468**, 803–806 (2010).
3. A. Sommers, H. Rajaram, M. Morlighem, SHAKTI: Subglacial hydrology and kinetic, transient interactions v1. 0. *Geosci. Model Dev.* **11**, 2955–2974 (2018).
4. M. Bougamont, S. Price, P. Christoffersen, A. Payne, Dynamic patterns of ice stream flow in a 3-D higher-order ice sheet model with plastic bed and simplified hydrology. *J. Geophys. Res. Earth Surf.* **116**, F04018 (2011).
5. S. Tulaczyk, B. Kamb, H. Engelhardt, Basal mechanics of Ice Stream B, West Antarctica: 2. Undrained plastic bed model. *J. Geophys. Res. Solid* **105**, 483–494 (2000).
6. W. Wei, D. D. Blankenship, J. S. Greenbaum, N. Gourmelen, C. F. Dow, T. G. Richter, C. A. Greene, D. A. Young, S. H. Lee, T. W. Kim, W. S. Lee, K. M. Assmann, Getz Ice Shelf melt enhanced by freshwater discharge from beneath the West Antarctic Ice Sheet. *Cryosphere* **14**, 1399–1408 (2020).
7. L. Li, A. R. Aitken, M. D. Lindsay, B. Kulessa, Sedimentary basins reduce stability of Antarctic ice streams through groundwater feedbacks. *Nat. Geosci.* **15**, 645–650 (2022).
8. C. Hofstede, P. Christoffersen, B. Hubbard, S. H. Doyle, T. J. Young, A. Diez, O. Eisen, A. Hubbard, Physical conditions of fast glacier flow: 2. Variable extent of anisotropic ice and soft basal sediment from seismic reflection data acquired on Store Glacier, West Greenland. *J. Geophys. Res. Earth* **123**, 349–362 (2018).
9. F. Walter, J. Chaput, M. P. Lüthi, Thick sediments beneath Greenland's ablation zone and their potential role in future ice sheet dynamics. *Geology* **42**, 487–490 (2014).
10. C. D. Gustafson, K. Key, M. R. Siegfried, J. P. Winberry, H. A. Fricker, R. A. Venturelli, A. B. Michaud, A dynamic saline groundwater system mapped beneath an Antarctic ice stream. *Science* **376**, 640–644 (2022).
11. F. H. King, Observations and experiments on the fluctuations in the level and rate of movement of groundwater on the Wisconsin Agricultural Experiment Station Farm and at Whitewater, Wisconsin, *US Department of Agriculture Bulletin* (Weather bureau, 1892), vol. 5.
12. M. Sophocleous, Interactions between groundwater and surface water: The state of the science. *Hydrgeol. J.* **10**, 52–67 (2002).
13. S. E. Ingebritsen, W. E. Sanford, C. Neuzil, *Groundwater in Geologic Processes*. (Cambridge Univ. Press, 2023).
14. C. Neuzil, Hydromechanical effects of continental glaciation on groundwater systems. *Geofluids* **12**, 22–37 (2012).
15. J.-M. Lemieux, E. Sudicky, W. Peltier, L. Tarasov, Dynamics of groundwater recharge and seepage over the Canadian landscape during the Wisconsinian glaciation. *J. Geophys. Res. Earth* **113**, F01011 (2008).
16. M. Person, J. McIntosh, V. Bense, V. Remenda, Pleistocene hydrology of North America: The role of ice sheets in reorganizing groundwater flow systems. *Rev. Geophys.* **45**, RG3007 (2007).
17. A. Provost, C. Voss, C. Neuzil, SITE-94 Glaciation and Regional Ground-Water Flow in the Fennoscandian Shield. Tech. Rep. 96:11, SKI Report, Stockholm, Sweden, 1997.
18. B. Smith, H. A. Fricker, A. S. Gardner, B. Medley, J. Nilsson, F. S. Paolo, N. Holschuh, S. Adusumilli, K. Brunt, B. Csatho, K. Harbeck, T. Markus, T. Neumann, M. Siegfried, H. Zwally, Pervasive ice sheet mass loss reflects competing ocean and atmosphere processes. *Science* **368**, 1239–1242 (2020).
19. N. Foley, S. M. Tulaczyk, D. Grombacher, P. T. Doran, J. Mikucki, K. F. Myers, N. Foged, H. Dugan, E. Auken, R. Virginia, Evidence for pathways of concentrated submarine groundwater discharge in east Antarctica from helicopter-borne electrical resistivity measurements. *Hydrology* **6**, 54 (2019).
20. K. Terzaghi, *Erdbaumechanik auf bodenphysikalischer Grundlage*. F. Deuticke, Wien (1925).
21. R. E. Gibson, The progress of consolidation in a clay layer increasing in thickness with time. *Geotechnique* **8**, 171–182 (1958).
22. J.-M. Lemieux, E. Sudicky, W. Peltier, L. Tarasov, Simulating the impact of glaciations on continental groundwater flow systems: 1. Relevant processes and model formulation. *J. Geophys. Res. Earth* **113**, F03017 (2008).
23. B. T. Gooch, D. A. Young, D. D. Blankenship, Potential groundwater and heterogeneous heat source contributions to ice sheet dynamics in critical submarine basins of East Antarctica. *Geochem. Geophys. Geosyst.* **17**, 395–409 (2016).
24. I. N. Otosaka, A. Shepherd, E. R. Ivins, N.-J. Schlegel, C. Amory, M. R. van den Broeke, M. Horwath, I. Joughin, M. D. King, G. Krinner, S. Nowicki, A. J. Payne, E. Rignot, T. Scambos, K. M. Simon, B. E. Smith, L. S. Sørensen, I. Velicogna, P. L. Whitehouse, G. A. C. Agosta, A. P.

Ahlstrøm, A. Blazquez, W. Colgan, M. E. Engdahl, X. Fettweis, R. Forsberg, H. Gallée, A. Gardner, L. Gilbert, N. Gourmelen, A. Groh, B. C. Gunter, C. Harig, V. Helm, S. A. Khan, C. Kittel, H. Konrad, P. L. Langen, B. S. Lecavalier, C.-C. Liang, B. D. Loomis, M. McMillan, D. Melini, S. H. Mernild, R. Mottram, J. Mouginot, J. Nilsson, B. Noël, M. E. Pattle, W. R. Peltier, N. Pie, M. Roca, I. Sasgen, H. V. Save, K.-W. Seo, B. Scheuchl, E. J. O. Schrama, L. Schröder, S. B. Simonsen, T. Slater, G. Spada, T. C. Sutterley, B. D. Vishwakarma, J. M. van Wessem, D. Wiese, W. van der Wal, B. Wouters, Mass balance of the Greenland and Antarctic ice sheets from 1992 to 2020. *Earth Syst. Sci. Data* **15**, 1597–1616 (2023).

25. H. Engelhardt, N. Humphrey, B. Kamb, M. Fahnestock, Physical conditions at the base of a fast moving Antarctic ice stream. *Science* **248**, 57–59 (1990).
26. R. Freeze, J. Cherry, *Groundwater*, (Prentice Hall, 1979).
27. J. Leeman, R. Valdez, R. Alley, S. Anandakrishnan, D. Saffer, Mechanical and hydrologic properties of Whillans Ice Stream till: Implications for basal strength and stick-slip failure. *J. Geophys. Res. Earth* **121**, 1295–1309 (2016).
28. F. Pattyn, Antarctic subglacial conditions inferred from a hybrid ice sheet/ice stream model. *Earth Planet. Sci. Lett.* **295**, 451–461 (2010).
29. J. Nilsson, A. S. Gardner, F. S. Paolo, Elevation change of the Antarctic Ice Sheet: 1985 to 2020. *Earth Syst. Sci. Data* **14**, 3573–3598 (2022).
30. A. Shepherd, D. J. Wingham, J. A. Mansley, Inland thinning of the Amundsen Sea sector, West Antarctica. *Geophys. Res. Lett.* **29**, 2-1–2-4 (2002).
31. The IMBIE team, Mass balance of the Antarctic Ice Sheet from 1992 to 2017. *Nature* **558**, 219–222 (2018).
32. J. S. Johnson, R. A. Venturelli, G. Balco, C. S. Allen, S. Braddock, S. Campbell, B. M. Goehring, B. L. Hall, P. D. Neff, K. A. Nichols, D. H. Rood, E. R. Thomas, J. Woodward, Review article: Existing and potential evidence for Holocene grounding line retreat and readvance in Antarctica. *Cryosphere* **16**, 1543–1562 (2022).
33. G. Balco, N. Brown, K. Nichols, R. A. Venturelli, J. Adams, S. Braddock, S. Campbell, B. Goehring, J. S. Johnson, D. H. Rood, K. Wilcken, B. Hall, J. Woodward, Reversible ice sheet thinning in the Amundsen Sea Embayment during the Late Holocene. *Cryosphere* **17**, 1787–1801 (2023).
34. R. A. Venturelli, B. Boehman, C. Davis, J. R. Hawkings, S. E. Johnston, C. D. Gustafson, A. B. Michaud, C. Mosbeux, M. R. Siegfried, T. J. Vick-Majors, V. Galy, R. G. M. Spencer, S. Warny, B. C. Christner, H. A. Fricker, D. M. Harwood, A. Leventer, J. C. Priscu, B. E. Rosenheim; SALSA Science Team, Constraints on the timing and extent of deglacial grounding line retreat in West Antarctica. *AGU Adv.* **4**, e2022AV000846 (2023).
35. D. P. Lowry, M. Krapp, N. R. Golledge, A. Alevropoulos-Borrill, The influence of emissions scenarios on future Antarctic ice loss is unlikely to emerge this century. *Commun. Earth Environ.* **2**, 1–14 (2021).
36. P. Christoffersen, M. Bougamont, S. P. Carter, H. A. Fricker, S. Tulaczyk, Significant groundwater contribution to Antarctic ice streams hydrologic budget. *Geophys. Res. Lett.* **41**, 2003–2010 (2014).
37. G. Catania, C. Hulbe, H. Conway, T. A. Scambos, C. Raymond, Variability in the mass flux of the Ross ice streams, West Antarctica, over the last millennium. *J. Glaciol.* **58**, 741–752 (2012).
38. L. Beem, S. Tulaczyk, M. King, M. Bougamont, H. Fricker, P. Christoffersen, Variable deceleration of Whillans Ice Stream, West Antarctica. *J. Geophys. Res. Earth* **119**, 212–224 (2014).
39. M. R. Siegfried, H. A. Fricker, S. P. Carter, S. Tulaczyk, Episodic ice velocity fluctuations triggered by a subglacial flood in West Antarctica. *Geophys. Res. Lett.* **43**, 2640–2648 (2016).
40. V. B. Spikes, B. M. Csatho, G. S. Hamilton, I. M. Whillans, Thickness changes on Whillans Ice Stream and Ice Stream C, West Antarctica, derived from laser altimeter measurements. *J. Glaciol.* **49**, 223–230 (2003).
41. R. Bindschadler, P. Vornberger, L. Gray, Changes in the ice plain of Whillans Ice Stream, West Antarctica. *J. Glaciol.* **51**, 620–636 (2005).
42. L. A. Stearns, K. C. Jezek, C. J. Van Der Veen, Decadal-scale variations in ice flow along Whillans Ice Stream and its tributaries, West Antarctica. *J. Glaciol.* **51**, 147–157 (2005).
43. D. MacAyeal, A low-order model of the Heinrich Event cycle. *Paleoceanography* **8**, 767–773 (1993).
44. A. Robel, E. DeGiuli, C. Schoof, E. Tziperman, Dynamics of ice stream temporal variability: Modes, scales and hysteresis. *J. Geophys. Res.* **118**, 925–936 (2013).
45. C. R. Meyer, A. A. Robel, A. W. Rempel, Frozen fringe explains sediment freeze-on during Heinrich events. *Earth Planet. Sci. Lett.* **524**, 115725 (2019).
46. K. Cuffey, W. Paterson, *The Physics of Glaciers*, (Pergamon, ed. 3, 2010).
47. G. S. Boulton, D. Dent, E. M. Morris, Subglacial shearing and crushing, and the role of water pressures in tills from south-east Iceland. *Geogr. Ann. Ser. B* **56**, 135–145 (1974).
48. K. Warburton, D. Hewitt, J. Neufeld, Tidal grounding-line migration modulated by subglacial hydrology. *Geophys. Res. Lett.* **47**, e2020GL089088 (2020).
49. A. Damsgaard, D. Egholm, J. Piotrowski, S. Tulaczyk, N. K. Larsen, C. Brædstrup, A new methodology to simulate subglacial deformation of water-saturated granular material. *Cryosphere* **9**, 2183–2200 (2015).
50. I. Kasmalkar, A. Damsgaard, L. Goren, J. Suckale, Shear variation at the ice-till interface changes the spatial distribution of till porosity and meltwater drainage. *J. Geophys. Res. Earth* **126**, e2021JF006460 (2021).
51. D. B. Stone, G. K. Clarke, R. G. Ellis, Inversion of borehole-response test data for estimation of subglacial hydraulic properties. *J. Glaciol.* **43**, 103–113 (1997).
52. C. E. Neuzil, A. M. Provost, Ice sheet load cycling and fluid underpressures in the Eastern Michigan Basin, Ontario, Canada. *J. Geophys. Res. Solid Earth* **119**, 8748–8769 (2014).
53. A. Burton-Johnson, R. Dziadek, C. Martin, Review article: Geothermal heat flow in Antarctica: Current and future directions. *Cryosphere* **14**, 3843–3873 (2020).
54. I. Joughin, S. Tulaczyk, J. L. Bamber, D. Blankenship, J. W. Holt, T. Scambos, D. G. Vaughan, Basal conditions for Pine Island and Thwaites Glaciers, West Antarctica, determined using satellite and airborne data. *J. Glaciol.* **55**, 245–257 (2009).
55. B. Van Liefferinge, F. Pattyn, Using ice-flow models to evaluate potential sites of million year-old ice in Antarctica. *Clim. Past* **9**, 2335–2345 (2013).
56. T. Uemura, M. Taniguchi, K. Shibuya, Submarine groundwater discharge in Lützow-Holm Bay, Antarctica. *Geophys. Res. Lett.* **38**, L08402 (2011).
57. L. C. Liljedahl, T. Meierbachtol, J. Harper, D. van As, J.-O. Näslund, J.-O. Selroos, J. Saito, S. Follin, T. Ruskeeniemi, A. Kontula, N. Humphrey, Rapid and sensitive response of Greenland's groundwater system to ice sheet change. *Nat. Geosci.* **14**, 751–755 (2021).
58. A. B. Michaud, M. L. Skidmore, A. C. Mitchell, T. J. Vick-Majors, C. Barbante, C. Turetta, W. Vangelder, J. C. Priscu, Solute sources and geochemical processes in subglacial lake Whillans, West Antarctica. *Geology* **44**, 347–350 (2016).
59. C. L. Davis, R. A. Venturelli, A. B. Michaud, J. R. Hawkings, A. M. Achberger, T. J. Vick-Majors, B. E. Rosenheim, J. E. Dore, A. Steigmeyer, M. L. Skidmore, M. L. Skidmore, J. D. Barker, L. G. Benning, M. R. Siegfried, J. C. Priscu, B. C. Christner; SALSA Science Team, Biogeochemical and historical drivers of microbial community composition and structure in sediments from Mercer Subglacial Lake, West Antarctica. *ISME Commun.* **3**, 8 (2023).
60. J. R. Hawkings, M. L. Skidmore, J. L. Wadham, J. C. Priscu, P. L. Morton, J. E. Hatton, C. B. Gardner, T. J. Kohler, M. Stibal, E. A. Bagshaw, A. Steigmeyer, J. Barker, J. E. Dore, W. B. Lyons, M. Tranter, R. G. M. Spencer; SALSA Science Team, Enhanced trace element mobilization by Earth's ice sheets. *Proc. Natl. Acad. Sci. U.S.A.* **117**, 31648–31659 (2020).
61. T. J. Vick-Majors, A. B. Michaud, M. L. Skidmore, C. Turetta, C. Barbante, B. C. Christner, J. E. Dore, K. Christianson, A. C. Mitchell, A. M. Achberger, J. A. Mikucki, J. C. Priscu, Biogeochemical connectivity between freshwater ecosystems beneath the West Antarctic Ice Sheet and the sub-ice marine environment. *Global Biogeochem. Cycles* **34**, e2019GB006446 (2020).
62. E. Rignot, Y. Xu, D. Menemenlis, J. Mouginot, B. Scheuchl, X. Li, M. Morlighem, H. Seroussi, M. V. den Broeke, I. Fenty, C. Cai, L. An, B. de Fleurian, Modeling of ocean-induced ice melt rates of five west Greenland glaciers over the past two decades. *Geophys. Res. Lett.* **43**, 6374–6382 (2016).
63. A. Jenkins, P. Dutrieux, S. S. Jacobs, S. D. McPhail, J. R. Perrett, A. T. Webb, D. White, Observations beneath Pine Island Glacier in West Antarctica and implications for its retreat. *Nat. Geosci.* **3**, 468–472 (2010).
64. Y. Nakayama, C. Cai, H. Seroussi, Impact of subglacial freshwater discharge on Pine Island Ice Shelf. *Geophys. Res. Lett.* **48**, e2021GL093923 (2021).
65. E. Mantelli, M. Haseloff, C. Schoof, Ice sheet flow with thermally activated sliding. Part 1: The role of advection. *Proc. R. Soc. A* **475**, 20190410 (2019).
66. S. Price, H. Conway, E. Waddington, R. Bindschadler, Model investigations of inland migration of fast-flowing outlet glaciers and ice streams. *J. Glaciol.* **54**, 49–60 (2008).
67. C. R. Meyer, A. S. Downey, A. W. Rempel, Freeze-on limits bed strength beneath sliding glaciers. *Nat. Commun.* **9**, 1–6 (2018).
68. C. Schannwell, R. Drews, T. A. Ehlers, O. Eisen, C. Mayer, F. Gillet-Chaulet, Kinematic response of ice-rise divides to changes in ocean and atmosphere forcing. *Cryosphere* **13**, 2673–2691 (2019).
69. J.-E. Lesemann, J. A. Piotrowski, W. Wysota, "Glacial curvilineations": New glacial landforms produced by longitudinal vortices in subglacial meltwater flows. *Geomorphology* **120**, 153–161 (2010).
70. F. S. Ng, Canals under sediment-based ice sheets. *Ann. Glaciol.* **30**, 146–152 (2000).
71. S. P. Carter, H. A. Fricker, M. R. Siegfried, Antarctic subglacial lakes drain through sediment-floored canals: Theory and model testing on real and idealized domains. *Cryosphere* **11**, 381–405 (2017).
72. A. Damsgaard, J. Suckale, J. A. Piotrowski, M. Houssais, M. R. Siegfried, H. A. Fricker, Sediment behavior controls equilibrium width of subglacial channels. *J. Glaciol.* **63**, 1034–1048 (2017).
73. I. Kasmalkar, E. Mantelli, J. Suckale, Spatial heterogeneity in subglacial drainage driven by till erosion. *Proc. R. Soc. A* **475**, 20190259 (2019).

74. J. Walder, A. Fowler, Channelized subglacial drainage over a deformable bed. *J. Glaciol.* **40**, 3–15 (1994).
75. B. de Fleurian, M. A. Werder, S. Beyer, D. J. Brinkerhoff, I. Delaney, C. F. Dow, J. Downs, O. Gagliardini, M. J. Hoffman, R. L. Hooke, J. Seguinot, A. N. Sommers, SHMIP The subglacial hydrology model intercomparison project. *J. Glaciol.* **64**, 897–916 (2018).
76. C. F. Dow, The role of subglacial hydrology in Antarctic ice sheet dynamics and stability: A modelling perspective. *Ann. Glaciol.*, 1–6 (2023).
77. J. Selker, N. van de Giesen, M. Westhoff, W. Luxemburg, M. B. Parlange, Fiber optics opens window on stream dynamics. *Geophys. Res. Lett.* **33**, L24401 (2006).
78. P. Lamontagne-Hallé, J. M. McKenzie, B. L. Kurylyk, S. C. Zipper, Changing groundwater discharge dynamics in permafrost regions. *Environ. Res. Lett.* **13**, 084017 (2018).
79. J. Gaona, K. Meinikmann, J. Lewandowski, Identification of groundwater exfiltration, interflow discharge, and hyporheic exchange flows by fibre optic distributed temperature sensing supported by electromagnetic induction geophysics. *Hydrol. Process.* **33**, 1390–1402 (2019).
80. W. Chu, D. M. Schroeder, H. Seroussi, T. T. Creyts, S. J. Palmer, R. E. Bell, Extensive winter subglacial water storage beneath the Greenland Ice Sheet. *Geophys. Res. Lett.* **43**, 12,484–12,492 (2016).
81. J. Z. Downs, J. V. Johnson, J. T. Harper, T. Meierbachtol, M. A. Werder, Dynamic hydraulic conductivity reconciles mismatch between modeled and observed winter subglacial water pressure. *J. Geophys. Res. Earth* **123**, 818–836 (2018).
82. H. Goelzer, S. Nowicki, A. Payne, E. Larour, H. Seroussi, W. H. Lipscomb, J. Gregory, A. Abe-Ouchi, A. Shepherd, E. Simon, C. Agosta, P. Alexander, A. Aschwanden, A. Barthel, R. Calov, C. Chambers, Y. Choi, J. Cuzzone, C. Dumas, T. Edwards, D. Felikson, X. Fettweis, N. R. Golledge, R. Greve, A. Humbert, P. Huybrechts, S. Le clec'h, V. Lee, G. Leguy, C. Little, D. P. Lowry, M. Morlighem, I. Nias, A. Quiquet, M. Rückamp, N.-J. Schlegel, D. Slater, R. Smith, F. Straneo, L. Tarasov, R. van de Wal, M. van den Broeke, The future sea-level contribution of the Greenland ice sheet: A multi-model ensemble study of ISMIP6. *Cryosphere* **14**, 3071–3096 (2020).
83. H. Seroussi, S. Nowicki, A. J. Payne, H. Goelzer, W. H. Lipscomb, A. Abe Ouchi, C. Agosta, T. Albrecht, X. Asay-Davis, A. Barthel, R. Calov, R. Cullather, C. Dumas, R. Gladstone, N. Golledge, J. M. Gregory, R. Greve, T. Hatterman, M. J. Hoffman, A. Humbert, P. Huybrechts, N. C. Jourdain, T. Kleiner, E. Larour, G. R. Leguy, D. P. Lowry, C. M. Little, M. Morlighem, F. Pattyn, T. Pelle, S. F. Price, A. Quiquet, R. Reese, N.-J. Schlegel, A. Shepherd, E. Simon, R. S. Smith, F. Straneo, S. Sun, L. D. Trusel, J. Van Breedam, R. S. W. van de Wal, R. Winkelmann, C. Zhao, T. Zhang, T. Zwinger, ISMIP6 Antarctica: A multi-model ensemble of the Antarctic ice sheet evolution over the 21st century. *The Cryosphere* **14**, 3033–3070 (2020).
84. H. S. Carslaw, J. C. Jaeger, Conduction of heat in solids. tech. rep., (Clarendon press, 1959).
85. J. Crank, P. Nicolson, A practical method for numerical evaluation of solutions of partial differential equations of the heat-conduction type, in *Mathematical proceedings of the Cambridge philosophical society*, (Cambridge, Univ. Press, 1947), vol. 43, pp. 50–67.

Acknowledgments: We thank M. Ranganathan, L. Zoet, V. Verjans, P. Christoffersen, and J. E. Christian for helpful conversations during the completion of this work and F. Pattyn and B. Van Liefferinge for sharing basal melt rate model output. Any use of trade, firm, or product names is for descriptive purposes only and does not imply endorsement by the U.S. Government. **Funding:** This work was supported by startup funds from the Georgia Tech Research Corporation (A.A.R. and S.J.S.) and NASA grant 80NSSC21K0912 (M.R.S.). **Author contributions:** Conceptualization: A.A.R., S.J.S., and C.D.G. Methodology: A.A.R., S.J.S., and C.M. Investigation: A.A.R. Visualization: A.A.R. and S.J.S. Writing: All authors. **Competing interests:** The authors declare that they have no competing interests. **Data and materials availability:** The code for the hydromechanical model and all Jupyter notebooks used to produce the figures in this study are archived in a persistent Zenodo repository located at https://doi.org/10.5281/zenodo.7951065. The hydromechanical model code is also available through an updated public GitHub repository located at https://github.com/aarobel/SubglacialExfiltration. All other data and information needed to evaluate the conclusions in the paper are present in the paper and the Supplementary Materials.

Submitted 28 February 2023
Accepted 19 July 2023
Published 18 August 2023
10.1126/sciadv.adh3693

ScienceAdvances

Contemporary ice sheet thinning drives subglacial groundwater exfiltration with potential feedbacks on glacier flow

Alexander A. Robel, Shi J. Sim, Colin Meyer, Matthew R. Siegfried, and Chloe D. Gustafson

Sci. Adv., **9** (33), eadh3693.
DOI: 10.1126/sciadv.adh3693

Science Advances (ISSN) is published by the American Association for the Advancement of Science. 1200 New York Avenue NW, Washington, DC 20005. The title *Science Advances* is a registered trademark of AAAS.